

Graphene nanoribbons on gold: Understanding superlubricity and edge effects

L Gigli,¹ N Manini,² A Benassi,³ E Tosatti,^{1,4} A Vanossi,^{5,1} R Guerra^{1,2}

¹International School for Advanced Studies (SISSA), Via Bonomea 265, 34136 Trieste, Italy

²Dipartimento di Fisica, Università degli Studi di Milano, Via Celoria 16, 20133 Milano, Italy

³Institute for Materials Science, Max Bergmann Center of Biomaterials, and Dresden Center for Computational Materials Science (DCCMS), TU Dresden, 01062 Dresden, Germany

⁴The Abdus Salam International Centre for Theoretical Physics (ICTP), Strada Costiera 11, 34151 Trieste, Italy

⁵CNR-IOM Democritos National Simulation Center, Via Bonomea 265, 34136 Trieste, Italy

E-mail: vanossi@sissa.it, guerra@sissa.it

Abstract. We address the atomistic nature of the longitudinal static friction against sliding of graphene nanoribbons (GNRs) deposited on gold, a system whose structural and mechanical properties have been recently the subject of intense experimental investigation. By means of numerical simulations and modeling we show that the GNR interior is structurally lubric (“superlubric”) so that the static friction is dominated by the front/tail regions of the GNR, where the residual uncompensated lateral forces arising from the interaction with the underneath gold surface opposes the free sliding. As a result of this edge pinning the static friction does not grow with the GNR length, but oscillates around a fairly constant mean value. These friction oscillations are explained in terms of the GNR-Au(111) lattice mismatch: at certain GNR lengths close to an integer number of the beat (or moiré) length there is good force compensation and superlubric sliding; whereas close to half odd-integer periods there is significant pinning of the edge with larger friction. These results make qualitative contact with recent state-of-the-art atomic force microscopy experiment, as well as with the sliding of other different incommensurate systems.

Keywords: graphene, nanoribbon, superlubricity, friction.

1. Introduction

When deposited on a clean flat crystal surface, nano-sized objects usually provide a well-defined mechanical contact. For this and other reasons, systems of this kind have been the subject of extensive nanofriction investigation in recent years both in experiments [1, 2, 3, 4, 5, 6, 7, 8, 9, 10, 11, 12] and in simulations [13, 14, 15, 16, 17, 18, 19, 20, 21, 22]. The gold-graphite interface constitutes an especially smooth and lubric contact, characterized by tenuous lateral forces, which make it an ideal workhorse system for basic tribological studies. In particular the controlled movements of gold and antimony nanoclusters deposited on the graphite surface provided elegant realizations of structural lubricity [23, 24], leading to interfaces with sliding friction forces growing sublinearly with the contact area [11, 10]. Unfortunately the control over gold nanocluster size and structure is, at best, statistical, and this limitation prevents a precise control of the interface geometry and orientation. More recent work focused on the specular, but better controlled, sliding of graphitic adsorbates, e.g., in the form of graphene nanoribbons (GNRs), on gold substrates, and in particular on the Au(111) surface [25, 26]. State-of-the-art on-surface synthesis techniques allow the construction of GNRs of controlled shape on the gold surface [25, 27], where size and orientation of the nano object can be monitored with atomic resolution by means of tip-scanning microscopy in clean conditions of ultra-high vacuum and low temperature. In addition, the tip of an atomic force microscope (AFM) can easily induce displacements of the GNRs on the surface, thanks to the very smooth GNR-gold interaction. These forced sliding displacements were exploited by Kawai *et al.* [26] to probe the frictional properties of this interface. That work has provided initial evidence for a weak length dependence of static friction, defined as the minimum external force needed to start the longitudinal sliding of the GNRs along their long direction. That data was however affected by large error bars, which prevented the clear-cut attribution of the frictional properties. An intervention of theory is therefore called for to clarify the ideal frictional behavior to be expected for these systems.

2. System and Methods

Mimicking the experimental geometry [26], we simulate armchair GNRs consisting of a stripe of alternating triplets and pairs of carbon hexagons, as sketched in Figure 1. The resulting GNR width is $\simeq 0.7$ nm, while for the GNR length L we investigate the experimentally significant range from $L \simeq 4.2$ nm (10 unit cells, $N_C = 140$ C atoms) to $L \simeq 60.3$ nm (144 unit cells, $N_C = 2016$ C atoms).

Our goal is to determine by simulation, and to explain by theory, the static friction force which resists the longitudinal sliding of these ribbons on gold. One complication of real gold (111) surfaces may be represented by reconstruction, both the primary ($22 \times \sqrt{3}$) reconstruction, and the secondary herringbone long-period one [28, 29, 30]. By ignoring these reconstructions (not always present), we extract the simplest and

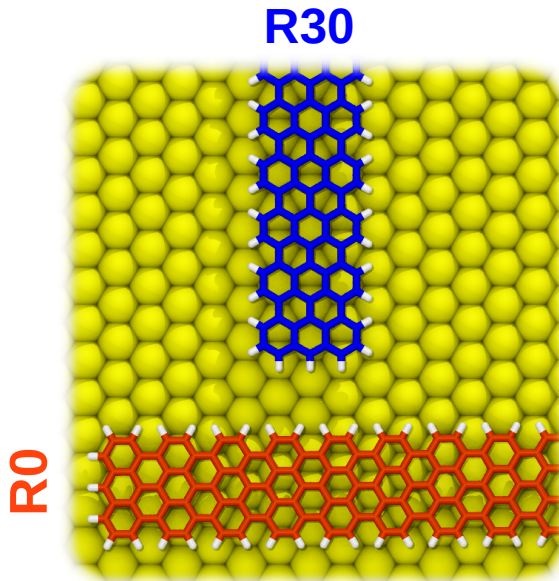


Figure 1. Top-view sketch of the R0 (orange) and R30 (blue) alignments of the GNR deposited on the Au(111) substrate (yellow). Broken carbon bonds at front, back, and side edges are passivated by hydrogen atoms (white).

fundamental length dependence of friction on unreconstructed Au(111), represented here by a rigid monolayer triangular lattice with spacing $a_{\text{Au}} = 288.38$ pm.

We investigate mainly two relative alignments of the GNR with the substrate: the R0 epitaxial orientation, in which the GNRs are aligned with the long axis parallel to Au[1, -2, 1] ($\theta = 0$), and the R30 orientation with the GNRs rotated by 30° (or equivalently 90°) relative to R0, namely along the Au[-1, 0, 1] direction ($\theta = 30^\circ$), see Figure 1. Within our model, depending on the GNR length, the R0 angular alignment turns out to be only weakly locally stable against global rotations, with an essentially flat $T = 0$ total energy landscape over an angular range of approximately $\theta \simeq \pm 5^\circ$. This flatness is probably due to the interplay and mutual cancellation of the spontaneous interface angular misalignment prescribed by the Novaco-McTague theory [31, 32, 33, 34, 35], that for a full graphene monolayer would demand an energy minimum at some small $\theta \neq 0$, and the finite size and elongated shape of the GNR overlayer, favoring perfect alignment at $\theta = 0$. In practice, while in the experiment of [26] the commonest GNR orientation is the R30 alignment, the R0 arrangement seems to be favored in the case of graphene flakes grown, with a different technique, on Au(111) [36]. It is also possible that for the GNRs of [26] the edges might play a role and tilt the tight energy balance in favor of the R30 orientation. Alternatively, the prevalence of R30 might be a purely kinetic effect of the synthesis method adopted for the GNR [25, 27]. With our model forces, and for large lengths L , the R30 orientation is a local energy minimum of marginally higher energy, approximately 0.008 meV/atom, relative to the R0 orientation. At any rate, we simulate the static friction of both orientations and compare the outcomes.

In our model, the GNR atomistic dynamics is determined by the force field based on the Reactive Empirical Bond Order (REBO) C-C and C-H interaction potential [37] as implemented in LAMMPS [38], plus a 2-body Lennard-Jones (LJ) potential describing the C-Au interaction. Following Refs. [39, 26] we take $\sigma_C = 274$ pm and $\varepsilon_C = 2.5$ meV for the C-Au LJ parameters, which is best adapted to model the mutual corrugation energy of graphitic materials with Au(111) when the latter is represented by a single rigid layer. As is generally the case in experiment, where broken bonds are immediately saturated, we assume all broken bonds of the peripheral C atoms to be H-passivated. Our tests proved that, even within an empirical force modeling where electrons are absent, the lack of H passivation, assumed earlier [26], would produce significantly shorter C-C bond lengths of the graphitic edge, thus compromising a realistic moiré superstructure as well as static friction which, as we shall see, is edge-related. The less important H-Au interaction is also described by a LJ potential with $\sigma_H = \sigma_C$ and $\varepsilon_H = 1.0$ meV. We verified that a variation, by a factor of 2 or 3, in ε_C and ε_H does not affect the overall trend of friction versus size, simply rescaling the overall static-friction curves almost rigidly by the same factor. We also verified that increasing the number of Au layers representing the fcc bulk structure of the gold substrate leads to relatively small changes in the model output, so that these changes can mostly be compensated by a small adaptation of the LJ C-Au and H-Au parameters to fit the experimentally observed frequency shifts profiles recorded during the AFM scans [26].

To obtain the fully relaxed initial configuration of each GNR on gold we run a Langevin simulated thermal annealing by decreasing the target temperature from $T = 50$ K down to 0 K in 300 ps, at a rate of -0.17 K/ps, and a subsequent damped relaxation at $T = 0$ for a further 200 ps. To prevent thermally-induced rotations of R0 GNRs during this annealing protocol, we cancel their out-of-plane angular momentum during the relaxation dynamics. In addition, the robustness of the relaxation procedure is tested against in-plane displacements of the initial center-mass position, adopting the resulting lowest-energy GNR arrangement as the fully relaxed initial configuration for the subsequent friction simulations.

Starting from these relaxed configurations, we then evaluate the static friction by means of zero-temperature molecular-dynamics (MD) simulations, by applying an adiabatically increasing external force F^{tot} directed along the GNR main axis. The force can be applied to the GNR center of mass or, it could be applied (as a pulling force), to the GNR leading edge. By directly testing that an edge-driven simulation protocol does not lead to fundamentally different outcomes, as expected for this kind of large material stiffness and small length size [40], we choose here a uniform center-of-mass driving of the GNR, with the same force $F = F^{\text{tot}}/N$ equally acting on all $N = (N_C + N_H)$ atoms of the adsorbate. Our protocol is to increase adiabatically F in small incremental steps $dF \simeq 8 \cdot 10^{-5}$ pN/atom, letting the system structure relax and the kinetic energy be absorbed after each step before the next. This relaxation procedure is implemented via a viscous damping rate η , whose specific value (here, 2 ps^{-1}), we checked, does not affect the outcome of the simulated tribological response. We finally estimate the static

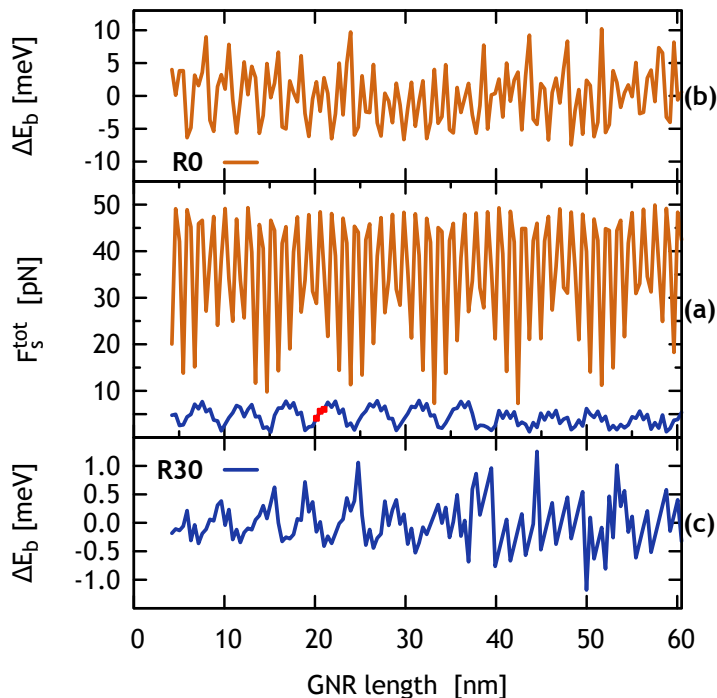


Figure 2. Dependence on the GNR length L of the computed total static friction force (a), and of the variation of the total adsorption free energy with respect to its linear fit (b) and (c). The GNR orientations are R0 (orange, $\theta=0$) and R30 (blue, $\theta=30^\circ$). The linear fits are $E_b = pL + q$, with $p = -345.735 / -345.891$ meV/nm and $q = -34.5197 / -21.1741$ meV for R0 / R30 respectively. Red symbols mark the values for the GNRs of Figure 5.

friction force F_s^{tot} as the smallest force F^{tot} leading to a freely sliding configuration, with the GNR center-mass speed experiencing a frank increase in the pulling direction exceeding 10^{-4} m/s in simulation.

3. Static friction

Figure 2a reports the total static friction force, F_s^{tot} , as a function of the GNR length for the R0 and R30 orientations. These results show that the R0-oriented GNRs exhibit a small static friction ($\sim 20 - 50$ pN), which nonetheless is always systematically larger compared to R30-oriented GNRs (~ 5 pN). Interestingly, for both orientations, Figure 2a displays periodic-like oscillations of F_s^{tot} as a function of L , without any systematic increase. Compatible with the experimental observations of [26], this result is consistent with a *per atom* $F_s = \text{const}/L$. Static friction per particle decreases as a function of the GNR length, indicating an asymptotically vanishing friction per unit area of contact, the characteristic hallmark of a superlubric tribological contact. For the graphene-gold interface, characterized by a fairly weak graphene-Au(111) interaction, very stiff in-plane C-C bonds, and mutually mismatched periodicities, one does indeed expect a structurally lubric behavior, which here emerges even for GNRs, finite-width graphene

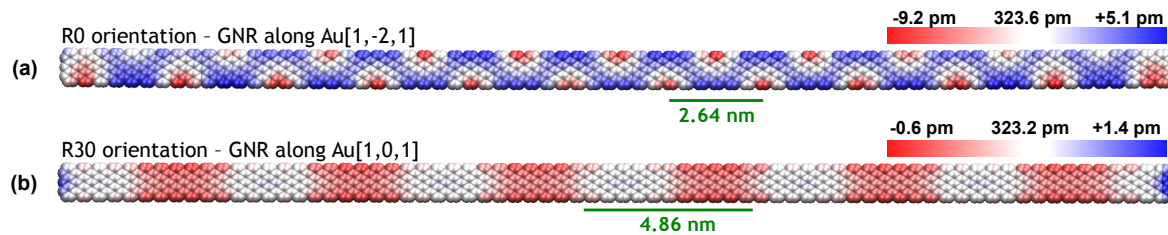


Figure 3. The relaxed GNR configuration of the 30 nm-long GNR in the R0 (a) and R30 (b) orientations relative to the underlying Au(111) surface (not shown). The color of the C atoms maps their vertical displacement relative to the GNR average height (passivating H atoms are not shown). The wavelength λ_m of the moiré pattern, as extracted from the lattice-mismatch value, is indicated for each orientation.

ribbons. The independence of the total static friction for the whole GNR from the length L shows that there is no term linearly proportional to the contact area, the very definition of superlubricity [24].

The observed oscillation of F_s^{tot} can be explained as a consequence of ribbon-specific moiré pattern induced by the lattice-spacing mismatch. Figure 3 shows typical moiré patterns, those of a 30 nm-long relaxed GNR physisorbed along both R0 and R30 orientations. Here the moiré gives rise to, and is mapped by, vertical displacements z of the individual C atoms. They are mapped in contrasting colors, exhibiting quasi-periodic color patterns whose average periods $\lambda_m^{\text{R0}} = 2.64$ nm and $\lambda_m^{\text{R30}} = 4.86$ nm are highlighted. Lower- z regions (red) contribute more, and higher up segments (blue) contribute less to the total (negative) binding energy E_b of the physisorbed GNR. Due to the overall periodicity of the moiré-pattern envelop, in the GNR “bulk” interior these oscillations compensate, so that, on average, E_b grows linearly with L . There remains a residual oscillating contribution ΔE_b to E_b , which depends on the length of the short terminating section, namely the GNR part exceeding an integer number of moiré average wavelengths λ_m . It is precisely this short residual section of the GNR, whose contribution to energetics does not grow with L , that dominates the static friction force F_s^{tot} . Indeed, periodically in L , the GNR terminations explore configurations ranging from a locally best matching (a minimum of ΔE_b , with larger F_s^{tot}) or compensated (equally weighting red/blue areas, generating a local maximum of ΔE_b , and a small F_s^{tot}) arrangement. The anticorrelation of F_s^{tot} with ΔE_b atom is illustrated by comparing the panels of Figure 2.

The moiré patterns arise out of the mismatch between the GNR lattice spacing, $a_{\text{GNR}} = 420.00$ pm, and the spacing of the gold surface being $a_{\text{Au}} = 499.49$ pm for R0, and $a_{\text{Au}} = 288.38$ pm for R30. The resulting mismatch ratios are $\rho_{\text{R0}} = 0.8408 \simeq 1$ and $\rho_{\text{R30}} = 1.4564 \simeq 3/2$, respectively. The wavelengths of the R0 and R30 moiré oscillation patterns [33, 41, 42, 43] are $\lambda_m^{\text{R0}} = a_{\text{GNR}}/(1 - \rho_{\text{R0}}) \simeq 2.64$ nm, and $\lambda_m^{\text{R30}} = a_{\text{GNR}}/(3 - 2\rho_{\text{R30}}) \simeq 4.82$ nm. For the R0 orientation, the oscillation period should be approximately $\lambda_m^{\text{R0}} \simeq 6 a_{\text{GNR}}$; however, the main friction oscillation observed in Figure 2a exhibits a period $\frac{1}{2}\lambda_m^{\text{R0}} \simeq 3 a_{\text{GNR}}$. The zig-zag nature of the R0 moiré patterns (see Figure 3) explains this discrepancy: only one half of the moiré period is relevant for assigning

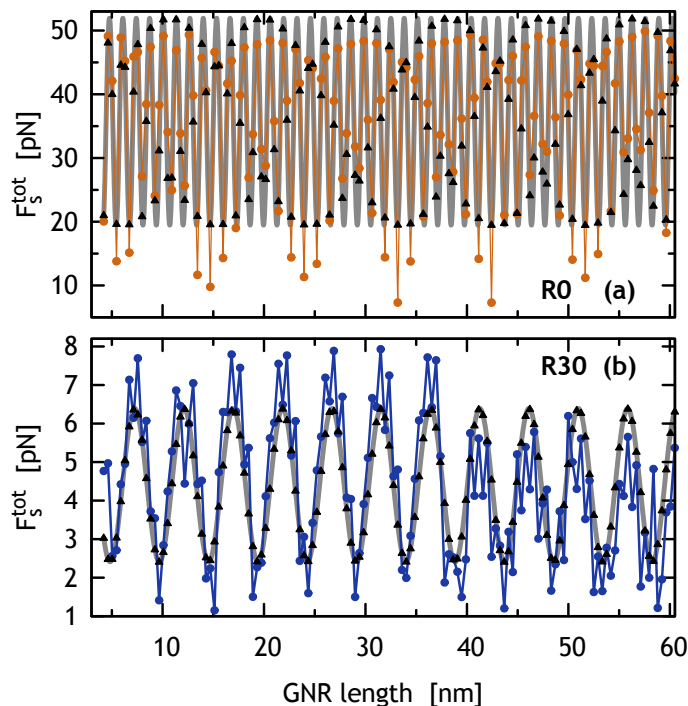


Figure 4. A comparison of the L -dependence of the total static friction force F_s (as in Figure 2a) for (a) R0 and (b) R30 orientation (circular dots), with the best-fitting curves of (1) (gray) evaluated at the lengths of actual GNRs (triangles).

the unbalanced pinned region at the end. For the R30 case, the moiré wavelength λ_m^{R30} accounts for the relatively slow oscillation in F_s^{tot} and ΔE_b displayed in the blue curves of Figure 2.

One can model the dependence of F_s with the GNR length L , as if it was solely related – as in a purely rigid system – to the uncompensated part of the moiré pattern of period λ_m [44, 45]. In the GNR, whose bulk is superlubric, this part is exclusively related to the nanoribbon edges – chiefly the front and the trailing edges, as the effect of the side edges for longitudinal applied driving turns out to be negligible. We can model this uncompensated length, and thus its contribution to the friction force, with a simple sinusoidal oscillation of period λ_m as a function of L [45]:

$$F(L) = \alpha + \beta \sin\left(\frac{2\pi L}{\lambda_m} - \delta\right), \quad (1)$$

where α , β , δ , and λ_m are fitting parameters. Figure 4 reports the curves of (1) best-fitting the F_s data of Figure 2a. For the R0 and R30 cases the fit yields $\lambda_m = 1.32$ nm and $\lambda_m = 4.86$ nm respectively, indeed matching the measured moiré nominal wavelengths (see Figure 3). The long-wavelength modulations seen for R0 in Figure 2a are now explained clearly by the simple sinusoidal fitting function of Figure 4a: these modulations are the trivial result of a poor sampling rate close to the Nyquist limit, an aliasing-type effect due to $\frac{1}{2}\lambda_m^{\text{R0}}$ being close, but not quite equal, to $3a_{\text{GNR}}$. In the R30 orientation, this effect is not visible since sampling is much denser, $\lambda_m \gg a_{\text{GNR}}$,

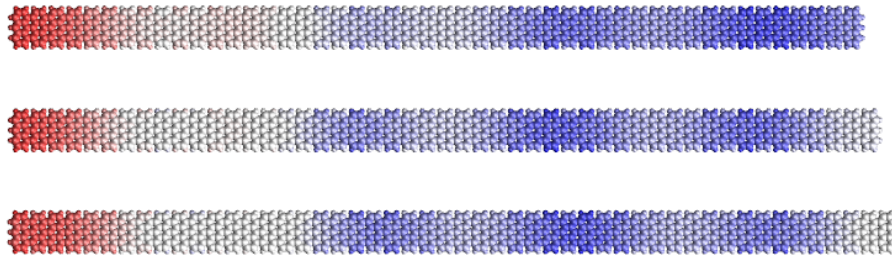


Figure 5. Colored strain maps for three R30 GNR of $L \simeq 20\text{--}20.8$ nm ($N_C = 672, 686, 700$), highlighted by red symbols in Figure 2a. The map portrays the atomic displacement component (red = small displacement, blue = large displacement) in the pulling-force direction, relative to the fully-relaxed initial configuration evaluated, for each GNR, under an uniform external force strength equaling 75% of the corresponding static friction threshold F_s^{tot} as reported in Figure 2a. While the central “bulk” GNR region clearly exhibits a large mobility, reflecting structural lubricity, shear resistance and pinning are localized at the nanoribbon ends (here, the GNR tails). The calculated static friction threshold turns out to be roughly proportional to the extension of this boundary red-blended region of the GNR, originating from the corresponding uncompensated part of the moiré superstructure of the relaxed configurations.

preventing any aliasing effect.

We note that the close correspondence of the nominal mismatch with the moiré “periodicities” in real systems can be perturbed by relaxation-induced strains and by thermal expansion. In the case of graphene, which exhibits a large in-plane stiffness, such strains are severely limited and will mainly influence only the higher-order approximants, i.e. large distances over which deformations tend to accumulate. In both cases, R0 and R30, deviations from this simple sinusoidal model can be attributed to the non-rigid nature of the simulated GNRs, and to the fact that the uncompensated GNR length does not contribute precisely as a sine of L . We have repeated the friction simulations with rigid GNRs, with the atomic reciprocal positions frozen in their configuration fully relaxed in vacuum, i.e. away from the gold surface. The computed F_s^{tot} values are indeed quite similar, with typical deviations of the order of 10%. One should not take the oscillating function of (1) as a serious model predicting the precise frictional force experienced by a GNR of a given length, but rather as a simple interpolating formula expressing the main message of the present work: the total static friction force needed to set a GNR in motion is totally edge-related, and does not grow with its length, but rather oscillates as the residual length of the end section of the GNR exceeding an integer number of moiré wavelengths.

As a confirmation that the main actors responsible for GNR friction are the end sections, responsible for the uncompensated part of the moiré pattern, Figure 5 shows the atomic displacements of the GNR atoms in the pulling direction when the applied driving has reached 75% of the depinning threshold of each of the three GNRs. In this picture, the red-colored regions are those resisting shear. These sections of $\sim \frac{1}{2}\lambda_m \simeq 1\text{--}2$ nm

near one or both of the GNR short ends (depending on the moiré of starting relaxed configuration) show up as the main responsible for GNR pinning. The blue-colored central “bulk” GNR region is ready to slide freely if it was not retained by the stiff elastic interaction with the pinned end section. It is therefore established that the short ends, the front end and the trailing end, represent the source of GNR pinning. Their relative effectiveness and positioning (front versus tail) depends on the GNR length in determining how well the matching conditions are realized at and near these edges. Similarly to what observed in other investigated tribological systems, yet with different geometries [41, 46, 47, 48, 49, 44, 45], we have a final confirmation that the approximately periodic oscillatory trend of F_s^{tot} as a function of L shown in Figure 2 is a consequence of the periodically varying size of the pinning end region.

4. Depinning

As soon as the pulling force exceeds the threshold F_s^{tot} , the GNR starts to move. While this depinning occurs uneventfully in the R30 orientation, we observe, interestingly, that the GNR initially aligned at R0 twists away from the $\theta=0$ orientation, choosing randomly a small (few degrees) clockwise or counterclockwise angle θ . While twisting, and subsequently in the depinned state, GNRs start to slide at an angle $\pm 30^\circ$ away from the pulling force, namely along one of the Au $[-1, 0, 1]$ directions, which is the same direction where R30-aligned GNRs are pulled. For the shorter GNRs, this twisting at depinning is an essentially rigid rotation, while it involves small but visible elastic deformations of GNRs with length $L > 30$ nm. The reason for this directional locking is that the small twist promotes the formation of 30° -oriented flat “channels” or “troughs” in the 2D translational energy profile for the center of mass of the GNR, which is then led to follow these channels where it encounters quite small barriers against sliding [50]. Experimentally, such predicted tendency to directional locking could be challenging to observe with an AFM, whose force cannot easily be applied to the center of mass. If observed, it would be remarkable.

5. Conclusion

We have presented a study of the static sliding friction of graphene nanoribbons on a metal surface, performed by classical MD simulations. Although with no pretense of quantitative predictive power, our model study appears to capture the essence of their depinning physics. Paralleling experimental results such as those by Kawai *et al.* [26], we find a small friction, strongly-oscillating and basically periodic with zero average increase upon increasing GNR length, supporting superlubricity in this system. The GNR static friction is entirely edge-related, whereas the GNR interior is superlubric, much like in a finite-size Frenkel-Kontorova chain [41, 46, 47], or in other incommensurate interfaces [48, 49, 44, 45]. Specifically, simulations allow us to correlate the periodicity of frictional oscillations to the characteristic length of the moiré pattern, and in particular

to the oscillating size of incomplete periods, namely the front and tail edges, which are responsible for the friction. This interpretation suggests that GNRs of certain “magic” lengths matching an integer number of moiré wavelengths λ_m could be selected for ultra-low-friction applications.

The twist-motion depinning of R0 GNRs induced by a directionally-locked sliding state and the dynamical frictional features observed experimentally with the GNRs either flat on the gold surface or with one end lifted up [26] are just a few of the problems calling for future investigation.

Acknowledgments

We acknowledge useful discussions with U. Duerig and E. Tentori. Work in Trieste was carried out under ERC Grant 320796 MODPHYSFRICT. The COST Action MP1303 is also gratefully acknowledged.

-
- [1] Bardotti L, Jensen P, Hoareau A, Treilleux M, Cabaud B, Perez A and Aires F C S 1996 *Surf. Sci.* **367** 276
 - [2] Dienwiebel M, Verhoeven G S, Pradeep N, Frenken J W M, Heimberg J A and Zandbergen H W 2004 *Phys. Rev. Lett.* **92** 126101
 - [3] Mougou K, Gnecco E, Rao A, Cuberes M T, Jayaraman S, McFarland E W, Haidara H and Meyer E 2008 *Langmuir* **24** 1577
 - [4] Dietzel D, Ritter C, Mönninghoff T, Fuchs H, Schirmeisen A and Schwarz U D 2008 *Phys. Rev. Lett.* **101** 125505
 - [5] Paolicelli G, Mougou K, Vanossi A and Valeri S 2008 *J. Phys.: Condens. Matter* **20** 354011
 - [6] Paolicelli G, Rovatti M, Vanossi A and Valeri S 2009 *Appl. Phys. Lett.* **95** 143121
 - [7] Schirmeisen A and Schwarz U D 2009 *ChemPhysChem.* **10** 2373
 - [8] Dietzel D, Feldmann M, Herding C, Schwarz U D and Schirmeisen A 2010 *Tribol. Lett.* **39** 273
 - [9] Dietzel D, Mönninghoff T, Herding C, Feldmann M, Fuchs H, Stegemann B, Ritter C, Schwarz U and Schirmeisen A 2010 *Phys. Rev. B* **82** 035401
 - [10] Brndiar J, Turanský R, Dietzel D, Schirmeisen A and Štich I 2011 *Nanotechnology* **22** 085704
 - [11] Dietzel D, Feldmann M, Schwarz U, Fuchs H and Schirmeisen A 2013 *Phys. Rev. Lett.* **111** 235502
 - [12] Feng X, Kwon S, Park J and Salmeron M 2013 *ACS Nano* **7** 1718
 - [13] Luedtke W D and Landman U 1999 *Phys. Rev. Lett.* **82** 3835
 - [14] Lewis L J, Jensen P, Combe N and Barrat J L 2000 *Phys. Rev. B* **61** 16084
 - [15] Maruyama Y 2004 *Phys. Rev. B* **69** 245408
 - [16] Pisov S, Tosatti E, Tartaglino U and Vanossi A 2007 *J. Phys.: Condens. Matter* **19** 305015
 - [17] Filippov A E, Dienwiebel M, Frenken J W M, Klafter J and Urbakh M 2008 *Phys. Rev. Lett.* **100** 046102
 - [18] Bonelli F, Manini N, Cadelano E and Colombo L 2009 *Eur. Phys. J. B* **70** 449
 - [19] Guerra R, Tartaglino U, Vanossi A and Tosatti E 2010 *Nature Mater.* **9** 634
 - [20] van Wijk M, Dienwiebel M, Frenken J and Fasolino A 2013 *Phys. Rev. B* **88** 235423
 - [21] Guerra R, Tosatti E and Vanossi A 2016 *Nanoscale* **8** 11108
 - [22] Sharp T, Pastewka L and Robbins M 2016 *Phys. Rev. B* **93** 121402
 - [23] Erdemir A and Martin J M (eds) 2007 *Superlubricity* (Elsevier, Amsterdam,)
 - [24] Vanossi A, Manini N, M, Urbakh, Zapperi S and Tosatti E 2013 *Rev. Mod. Phys.* **85** 529
 - [25] Ruffieux P, Wang S, Yang B, Sánchez-Sánchez C, Liu J, Dienel T, Talirz L, Shinde P, Pignedoli C A, Passerone D, Dumslaff T, Feng X, Müllen K and Fasel R 2016 *Nature* **531** 489

- [26] Kawai S, Benassi A, Gnecco E, Söde H, Pawlak R, Feng X, Müllen K, Passerone D, Pignedoli C A, Ruffieux P, Fasel R and Meyer E 2016 *Science* **351** 957
- [27] Jacobberger R M, Kiraly B, Fortin-Deschenes M, Levesque P L, McElhinny K M, Brady G J, Delgado R R, Roy S S, Mannix A, Lagally M G, Evans P G, Desjardins P, Martel R, Hersam M C, Guisinger N P and Arnold M S 2015 *Nature Comm.* **6** 8006
- [28] Wöll C, Chiang S, Wilson R J and Lippel P H 1989 *Phys. Rev. B* **39** 7988
- [29] Barth J V, Brune H, Ertl G and Behm R J 1990 *Phys. Rev. B* **42** 9307
- [30] Fujita D, Amemiya K, Yakabe T, Nejoh H, Sato T and Iwatsuki M 1997 *Phys. Rev. Lett.* **78** 3904
- [31] Novaco A and McTague J 1977 *Phys. Rev. Lett.* **38** 1286
- [32] McTague J and Novaco A 1979 *Phys. Rev. B* **19** 5299
- [33] Grey F and Bohr J 1992 *Europhys. Lett.* **18** 717
- [34] Mandelli D, Vanossi A, Manini N and Tosatti E 2015 *Phys. Rev. Lett.* **114** 108302
- [35] Mandelli D, Vanossi A, Invernizzi M, Paronuzzi S, Manini N and Tosatti E 2015 *Phys. Rev. B* **92** 134306
- [36] Wofford J M, Starodub E, Walter A L, Nie S, Bostwick A, Bartelt N C, Thürmer K, Rotenberg E, McCarty K F and Dubon O D 2012 *New J. Phys.* **14** 053008
- [37] Brenner D W, Shenderova O A, Harrison J A, Stuart S J, Ni B and Sinnott S B 2002 *J. Phys.: Condens. Matter* **14** 783
- [38] Plimpton S 1995 *J. Comput. Phys.* **117** 1
- [39] Nie S, N, Bartelt C, Wofford J M, Dubon O D, McCarty K F and Thürmer K 2012 *Phys. Rev. B* **85** 205406
- [40] Ma M, Benassi A, Vanossi A and Urbakh M 2015 *Phys. Rev. Lett.* **114** 055501
- [41] Floría L and Mazo J 1996 *Adv. Phys.* **45** 505
- [42] Vanossi A, Manini N, Divitini G, Santoro G and Tosatti E 2006 *Phys. Rev. Lett.* **97** 056101
- [43] Yankowitz M, Xue J, Cormode D, Sanchez-Yamagishi J, Watanabe K, Taniguchi T, Jarillo-Herrero P, Jacquod P and LeRoy B 2012 *Nature Phys.* **8** 382
- [44] Koren E and Duerig U 2016 *Phys. Rev. B* **93** 201404
- [45] Koren E and Duerig U 2016 *Phys. Rev. B* **94** 045401
- [46] Braun O M and Kivshar Y S 2004 *The Frenkel-Kontorova Model: Concepts, Methods, and Applications* (Springer, Berlin)
- [47] Cesaratto M, Manini N, Vanossi A, Tosatti E and Santoro G E 2007 *Surf. Sci.* **601** 3682
- [48] Varini N, Vanossi A, Guerra R, Mandelli D, Capozza R and Tosatti E 2015 *Nanoscale* **7** 2093
- [49] Pierno M, Bruschi L, Mistura G, Paolicelli G, di Bona A, Valeri S, Guerra R, Vanossi A and Tosatti E 2015 *Nature Nanotech.* **10** 714
- [50] Tentori E 2017 *Energetica di un nastro di grafene nanoscopico depositato su Au(111), al variare di posizione e allineamento angolare* Master's thesis University Milan URL <http://materia.fisica.unimi.it/manini/theses/tentori.pdf>